J Mater Sci (2009) 44:1141–1158
DOI 10.1007/s10853-008-3125-9

REVIEW

A review of mechanical properties of lead-free solders for electronic packaging

Hongtao Ma · Jeffrey C. Suhling

Received: 1 July 2008 / Accepted: 20 November 2008 / Published online: 27 January 2009
© Springer Science+Business Media, LLC 2009

Abstract The characterization of lead-free solders, especially after isothermal aging, is very important in order to accurately predict the reliability of solder joints. However, due to lack of experimental testing standards and the high homologous temperature of solder alloys ($T_h > 0.5T_m$ even at room temperature), there are very large discrepancies in both the tensile and creep properties provided in current databases for both lead-free and Sn–Pb solder alloys. Some recent researches show that the room temperature aging has significant effects on mechanical properties of solders. This paper is intended to review all available data in the field and give rise to the possible factors including room temperature effects which causes the large discrepancies of data. This review of the research literatures has documented the dramatic changes that occur in the constitutive and failure behavior of solder materials and solder joint interfaces during isothermal aging. However, these effects have been largely ignored in most previous studies involving solder material characterization or finite element predictions of solder joint reliability during thermal cycling. It is widely acknowledged that the large discrepancies in measured solder mechanical properties from one study to another arise due to differences in the microstructures of the tested samples. This problem is exacerbated by the aging issue, as it is clear that the microstructure and material behavior of the samples used in even a single investigation are moving targets that change rapidly even at room temperature. Furthermore, the effects of aging on solder behavior must be better understood so that more accurate viscoplastic constitutive equations can be developed for SnPb and SAC solders. Without such well-defined relationship, it is doubtful that finite element reliability predictions can ever reach their full potential.

H. Ma (✉) · J. C. Suhling
Auburn University, Auburn, AL 36849, USA
e-mail: hongtaoma@hotmail.com

General review of lead-free solders and the mechanical properties of lead-free solders

Lead-free solders in electronics

The use of solder alloys as metal joint materials can be dated back to thousands of years. With the emergence of the modern electronic packaging technology over the last few decades, solder alloys have been used as the interconnecting material in electronic packaging. Solder joints provide both the electrical connection and mechanical support in electronic packaging modules.

Eutectic or near eutectic tin/lead (Sn–Pb) solder (melting temperature $T_M = 183$ °C) has long been the predominant choice of the electronics industry due to its outstanding solderability and reliability. However, legislation that mandates the removal of lead from electronics has been actively pursued in the European Union and worldwide during the last 15 years due to environmental and health concerns regarding the high lead content in eutectic Sn–Pb solder. Lead is a proven toxic substance which can cause a range of negative impacts to both the environment and the human body [1]. Due to the current rapid improvements in electronic technology and the high cost of recycling processes, the recycling rate of electronic devices is very low, especially for high technology products, such as computers. It has been reported that less than 2% of the computers produced were recycled in 1998 [2]. The majority of the used electronics will end up in landfills

where the lead content will eventually leach out into the soil and hence the local ecosystem.

The European Union is particularly aggressive in pursuing the banning of lead from electronics. In June 2000, the EU adopted two directives, the Waste of Electrical and Electronic Equipment (WEEE) and the Directive of the Restriction of the Use of Certain Hazardous Substances (RoHS) [3]. The WEEE directive requires that lead has to be removed from any end-of-life electrical or electronic components. The RoHS specifically bans lead from electrical and electronic components manufactured after July 1, 2006. As a result of the enforcement of the directives, all electrical or electronic equipment and devices produced in or imported to EU member states must comply with these lead-free standards except those items that are exempted from the bans.

In Japan, although there is no specific government ban of lead in electronic components, in 1998, the advisory committee of Japan Institute of Electronics Industry Development Association (JEIDA) put forward a roadmap for the commercialization of lead-free solders (http://www.jeita.or.jp/english/press/2002/1217/attached.htm), and recommended lead-free alternatives for industry. The electronic industry in Japan is very active in pursuing lead-free products and many companies have brought their lead-free products into the market much earlier than the EU directives' effective dates [1, 4], including Panasonic in 2001, Sony in 2001: Toshiba in 2000, NEC in 2002, and Hitachi in 2001.

In the United States, there is again no specific government ban of lead from electrical and electronic devices. However, the U.S. Environmental Protection Agency (EPA) has listed lead among the top 17 chemicals that pose the greatest threat to human health [1]. The IPC (formerly known as the Institute of Interconnecting and Packaging Electrical Circuits) has also developed a roadmap for the lead-free movement in the U.S. [5]. The roadmap is designed to encourage both industry and academic institutes to actively research and develop lead-free assembly processes and to be prepared to respond to the worldwide lead-free movement. In recent years, many U.S. companies, including Motorola, Cisco, and Intel, have also been actively pursuing lead-free products in order to protect their world-wide market shares. Many universities have also been actively funding lead-free related research.

Other countries, such as China and South Korea, which are emerging electronic manufacturing bases, have also adopted directives similar to those of the European Union. Although the implementation deadlines and products covered by such legislation continue to evolve worldwide, it is clear that laws requiring the conversion to lead-free electronics are becoming a reality worldwide. Other factors that are affecting the push towards the elimination of lead in electronics are the market differentiation and advantage being realized by companies producing so-called "green" products that are lead-free. The companies that first successfully move into lead-free products will have a definite "first move" advantage over their competitors, which in today's competitive markets translates to profits and survival.

Lead-free solders

Overview

To be considered an alternative to Sn–Pb solder, lead-free candidates should have similar or better properties and reliability to those possessed by eutectic or near eutectic Sn–Pb solders. According to recent reports [6, 7], Pb in solders contributes outstanding properties to the overall reliability of the Sn–Pb solder, such as the following:

- Pb reduces the surface tension of pure tin to improve the wetting ability.
- Pb enables tin and copper to rapidly form intermetallic compounds by diffusion.
- Pb provides ductility to Sn–Pb solders.
- the addition of Pb prevents the transformation of β-tin to α-tin. If the transformation occurs, it will cause dramatic volume increase and loss of structural integrity and hence a loss of reliability. The β-tin to α-tin transformation in lead-free solders is also called "tin pest" or "tin disease." Karlya et al. observed significant "tin pest" phenomena in their lead-free solder specimens [8].
- Sn–Pb solders have a low melting temperature of 183 °C for eutectic solder, which allows the use of a low reflow temperature in the electronic packaging process and ensures the reliability of the packages.

Besides all of the above benefits of Pb, the cost of Pb is also low and it is very abundant. However, Pb is toxic, which causes the pressure from legislations worldwide.

Lee proposed some basic criteria for "perfect" lead-free alternatives [9]. The lead-free solder needs to have a similar melting temperature to existing Sn–Pb solders, particularly eutectic and near eutectic solders, in order to have a similar reflow profile during the manufacturing process; good wetting ability to ensure good metallization in the manufacturing process; the same or better electrical properties to efficiently transmit the electrical signals; and adequate mechanical properties, such as creep and fatigue, to preserve the reliability of the electronic packaging products. The new lead-free solders also need to be nontoxic and relatively inexpensive.

A great deal of research is currently underway in the lead-free solder area, including projects organized by consortia

including the High Density Packaging Users Group (HDPUG), the National Center for Manufacturing Sciences (NCMS), the National Institute for Standard and Technology (NIST), the International Electronics Manufacturing Initiative (iNEMI), and the Japan Electronic Industry Development Association (JEIDA). Although no "drop in" replacement has been identified that is suitable for all applications, Sn–Ag, Sn–Ag–Cu (SAC), and other alloys involving elements such as Sn, Ag, Cu, Bi, In, and Zn have been identified as promising replacements for standard 63Sn–37Pb eutectic solder. Several SAC alloys have been proposed by industrial consortiums. These include 96.5Sn–3.0Ag–0.5Cu (SAC 305) in Japan, 95.5Sn–3.8Ag–0.7Cu (SAC 387) in the EU, and 95.5Sn–3.9Ag–0.6Cu (SAC 396) in the USA. In addition, 95.5Sn–4.0Ag–0.5Cu (SAC405) has been widely adopted as an alloy for use in BGA solder joints. The main benefits of the various SAC alloy systems are their relatively low melting temperatures compared with the 96.5Sn–3.5Ag binary eutectic alloy, as well as their superior mechanical and solderability properties when compared to other lead-free solders. A survey conducted by Soldertec shows approximately 70% of the market for reflowing lead-free solders are in the SAC series (Fig. 1) [10]. There are some major challenges for the current series of lead-free solders. SAC series alloys have a higher melting temperature, around 217 °C, compared to 183 °C for the eutectic Sn–Pb solders. They thus require higher reflow temperature during the manufacturing process, which lead to reliability problems. The excessive build up of intermetallics formed at the interface between the solder joints and the copper pad can cause reliability problems. High costs are another issue for lead-free solders. As shown in Table 1 [6], the price of Ag is 150 times higher than that of Pb, and Cu is twice the price of Pb. Even though the Ag and Cu content is very low, the overall price of lead-free solders will inevitably be much higher than that of Sn–Pb. A typical SAC solder is reported to be over twice the price of the Sn–Pb eutectic solders [6]. The only good news about cost is that using SAC alloys will reduce the recycling cost by $0.13/kg, which will also increase the overall electronics recycling rate in the future [11]. Regardless all of these problems, the SAC series lead-free solders have been widely accepted by both industry and academic institutions. However, unless a "perfect" lead-free solder is found to replace the Sn–Pb series solders, research into new lead-free solders will continue for years to come.

Table 1 Cost of basic solder elements [6]

Metal element	Cost (US$/kg)
Lead	1.10
Zinc	1.08
Copper	2.24
Antimony	2.64
Bismuth	7.15
Tin	8.67
Silver	153.19
Indium	194.59

Sn–Ag–Cu lead-free solders series

Of the many lead-free solder series proposed in the last decade or so, Sn–Ag–Cu (SAC) series alloys have emerged as the most widely accepted (Fig. 1). Soldertec's survey shows that the most popular SAC are the near eutectic SAC alloys [10], which consist of 3.0–4.0% of Ag and 0.5–1.0% of Copper (Fig. 2). The melting point of these near eutectic SAC alloys is 217 °C, which is lower than the 96.5Sn–3.5Ag binary eutectic alloy at 221 °C. In the SAC system, the addition of Cu both lowers the melting temperature and improves the wettability [12].

Figure 3 shows a typical 3-D ternary phase diagram. The contours on the top surfaces of the figure represent the

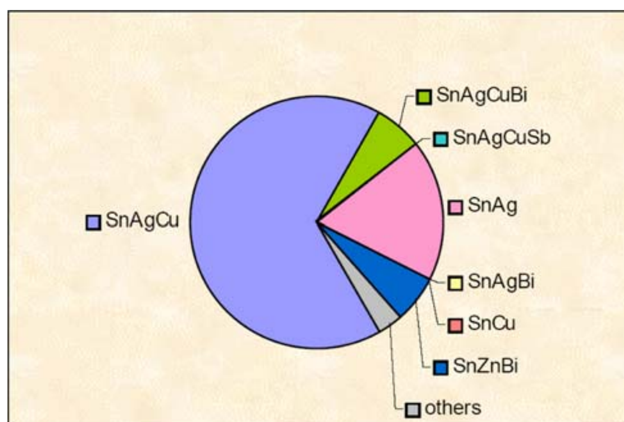

Fig. 1 The market share of different lead-free solders [10]

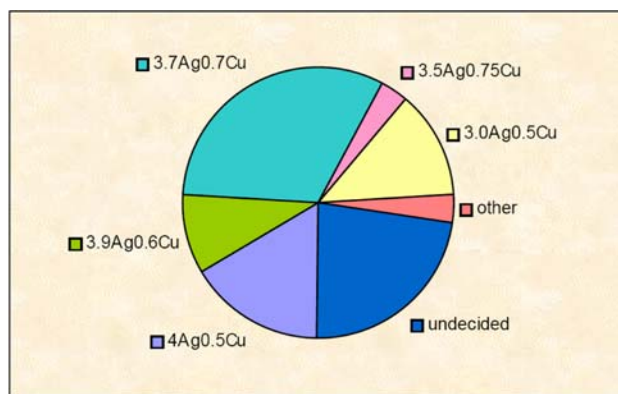

Fig. 2 Survey of the market share of different types of SAC alloys [10]

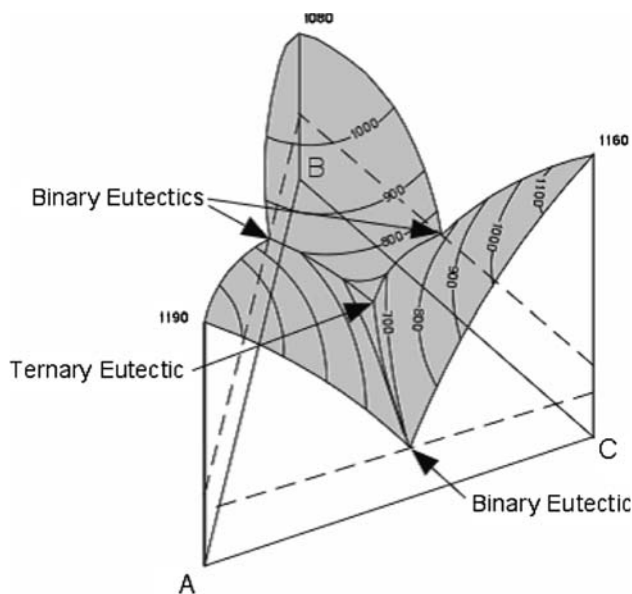

Fig. 3 Typical 3-D ternary phase diagram (http://www.tulane.edu/~sanelson/geol212/ternaryphdiag.htm)

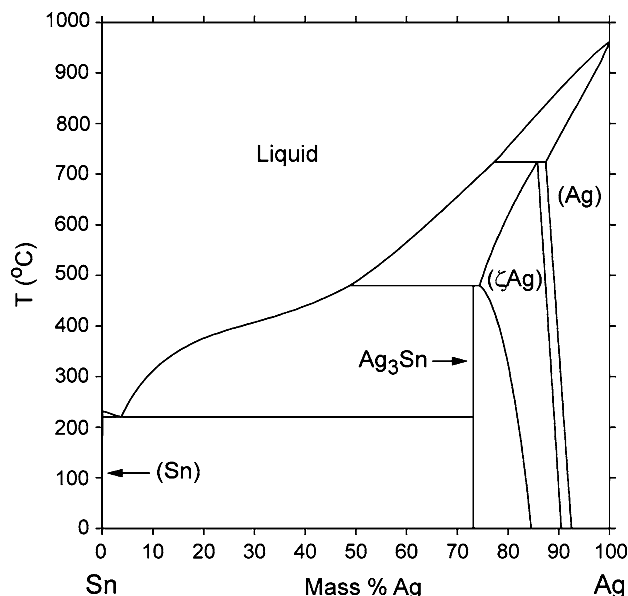

Fig. 5 Sn–Ag binary phase diagram (http://www.metallurgy.nist.gov/phase/solder/solder.html)

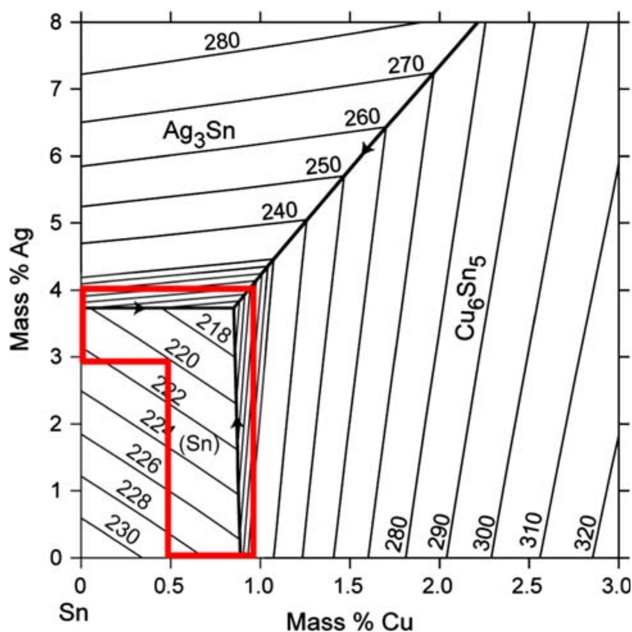

Fig. 4 Sn–Ag–Cu ternary phase diagram (http://www.metallurgy.nist.gov/phase/solder/solder.html)

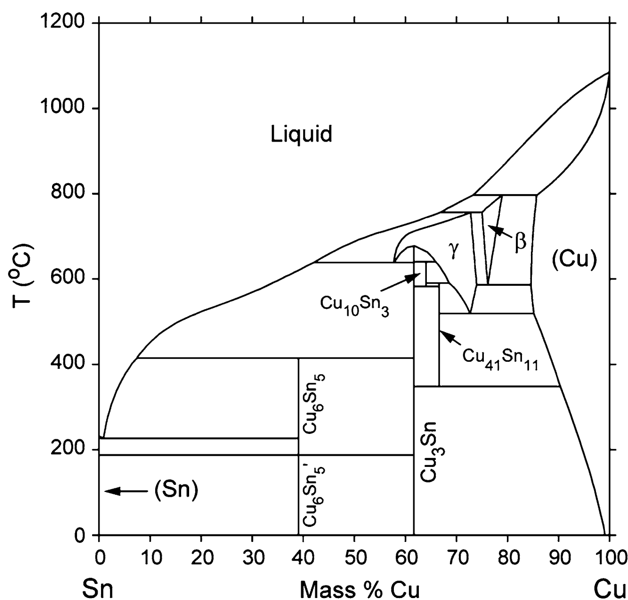

Fig. 6 Sn–Cu binary phase diagram (http://www.metallurgy.nist.gov/phase/solder/solder.html)

isothermal lines. Each of the three sectors represents the binary phase diagram of two of the three elements. The center of the diagram, where the isothermal lines reach the common, lowest point, is the eutectic point of the ternary system (http://www.tulane.edu/~sanelson/geol212/ternaryphdiag.htm). Figure 4 is the top view (2-D) of the ternary phase diagram of Sn–Ag–Cu.

The area indicated in the red box is the near eutectic region. Most of the SAC alloy compositions currently in the market are within this region. The eutectic and near eutectic melting temperature has been determined to be 217 °C, although the precise eutectic point is not known [12].

In SAC alloys, the formation of intermetallic compounds between the primary elements Sn and Ag, and Cu affect all the properties of the alloys. According to the binary phase diagram shown in Figs. 5, 6 and 7, there are three possible intermetallic compounds that may be formed: Ag_3Sn forms due to the reaction between Sn and

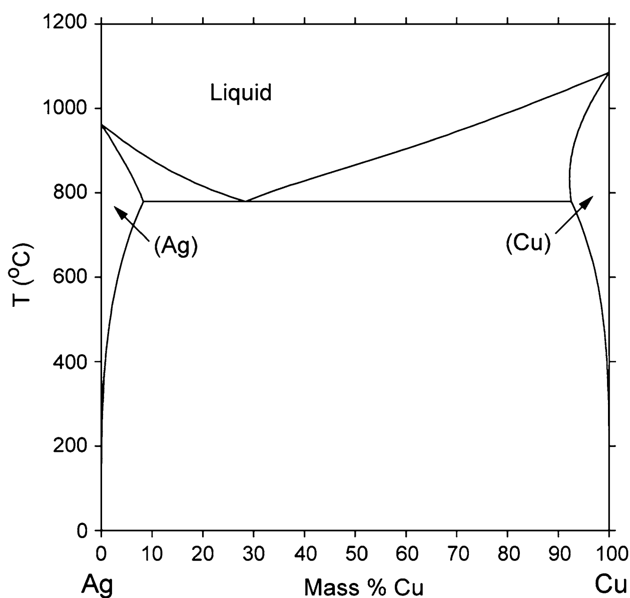

Fig. 7 Ag–Cu binary phase diagram (http://www.metallurgy.nist.gov/phase/solder/solder.html)

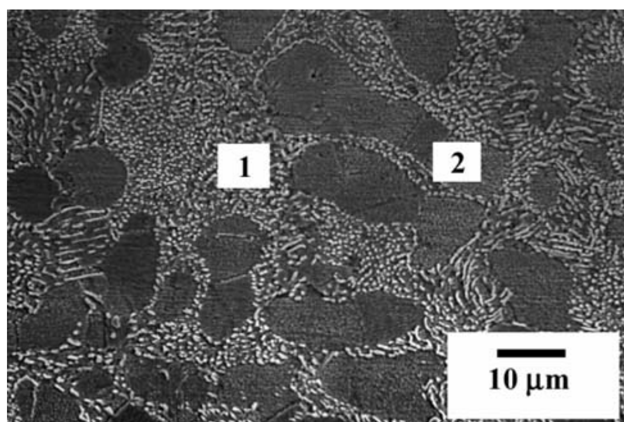

Fig. 8 Microstructure of typical SAC Alloys [13]

Ag (Fig. 5) and Cu_6Sn_5 forms due to the Sn and Cu reaction (Fig. 6), but Cu_3Sn will not form at the eutectic point unless the Cu content is high enough for the formation of Cu_3Sn at higher temperatures, so in bulk specimens Cu_3Sn is not present. Ag can also react with Cu to form Ag rich α phase and Cu rich β phase (Fig. 7). However, there is no reaction between Ag and Cu to form any kind of intermetallic compounds. Figure 8 shows a typical SAC structure with eutectic Sn matrix (2 in the figure) with Ag_3Sn (1 in the figure) intermetallic compounds [13]. The particles of intermetallic compounds possess much higher strength than the bulk material [14, 15]. Fine intermetallic particles in the Sn matrix can therefore strengthen the alloys. The intermetallic compounds can also improve the fatigue life of the solders, as SAC alloys are reported to have 3–4 times better fatigue properties than the Sn–Pb eutectic solders [16]. The higher fatigue resistance is believed to be contributed by the interspersed Ag_3Sn and Cu_6Sn_5 particles, which pin and block the movement of dislocations [16]. The many patents that have been granted for SAC systems have limited their use and hindered research on several of the SAC alloys, but fortunately the alloy Sn–4.0Ag–0.5Cu has not been patented [17].

Mechanical properties

In addition to conducting electricity, solder joints provide mechanical support for electronic devices. The mechanical properties of solder alloys are therefore critically important in producing reliable products. In determining the mechanical properties of solders, tensile properties and creep are of particular concern and have thus been most intensively investigated.

Tensile properties

Tensile properties are generally described by stress–strain curves. In engineering practice *engineering stress* and *engineering strain* are defined as follows [18]:

$$\sigma = \frac{P}{A_0} \quad (1)$$

$$\varepsilon = \frac{l_f - l_0}{l_0} \quad (2)$$

where P is the load, A_0 is the initial cross-sectional area, l_f is the final gage length, and l_0 is the initial gage length.

As shown in Fig. 9, a typical engineering stress–strain curve for solder alloys consists of an elastic region and a plastic region. In the elastic region, the engineering stress is linear, with the engineering strain conforming to Hooke's law as follows [19]:

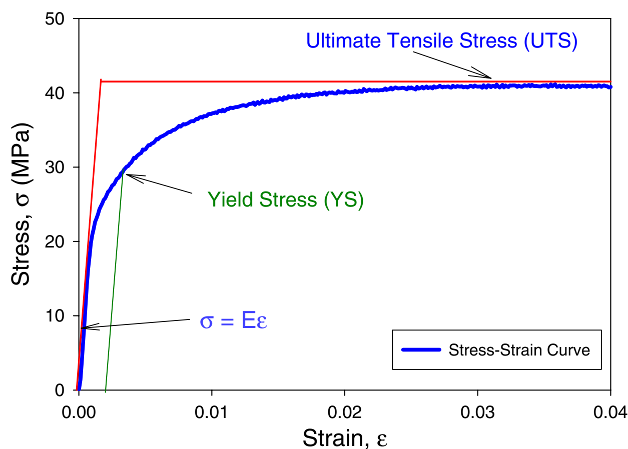

Fig. 9 Typical stress–strain curve of lead-free solders

$$\sigma = E\varepsilon \quad (3)$$

E is the elastic modulus (Young's modulus), which can be determined from the slope of the elastic portion of the stress–strain curve, σ is the engineering stress, and ε is the engineering strain. In the elastic region, if the load is removed the specimen can return to its original dimensions.

There is a wide range of values for the elastic modulus for different materials. Hertzberg described that the modulus of elasticity corresponds to the interatomic forces between adjacent atoms [18]. Gilman showed that the elastic modulus is inversely proportional to a power of the equilibrium adjacent atom distance X_0 as follows [20]:

$$E \propto \frac{1}{(X_0)^n} \quad (4)$$

Thus, when the distance between the atoms is larger the elastic modulus will be smaller. Ralls et al. showed that the elastic modulus of metal will decrease with increasing temperature [21]. The underlying reason for this is because the distance between adjacent atoms increases at higher temperatures. In engineering practice, the value of the elastic modulus obtained from the slope of the stress–strain curve is the static modulus, which is generally referred as the apparent or effective elastic modulus and also includes small inelastic deformations or time-dependent deformations such as creep. The apparent elastic modulus is usually smaller than the dynamic modulus measured by the acoustic or ultrasonic wave method, which largely eliminates the inelastic deformation due to rapid wave propagation [22–24].

When the load is high enough to exceed the elastic limits, the material will experience plastic deformation, which is permanent. Specimens subject to plastic deformation will simultaneously elongate and decrease in diameter. The Yield Stress (YS) is defined as just enough stress to cause the onset of plastic deformation. However, YS is difficult to determine. In engineering practice, a specified small amount of plastic deformation is used, with 0.2% being the widely accepted value [18]. This is determined by a parallel line drawn at 0.2% of the strain to the elastic slope (Fig. 9). When the load is removed at a point above the yield stress, the stress–strain curve will be approximately parallel to the initial modulus. The Ultimate Tensile Stress (UTS) is the maximum stress level that the material can withstand before failure under uniaxial loading.

Creep of solders

Electronic packaging components constantly experience stresses due to Coefficient of Thermal Expansion (CTE) mismatches in the packaging modules. Creep deformation is one of the major failure modes of solder joints for various electronic packaging modules due to its high homologous temperature [25]. The homologous temperature is the ratio of the temperature of the material and its melting temperature in degrees Kelvin [26].

$$T_h = \frac{T}{T_m} \quad (5)$$

The homologous temperature is an empirical value. When T_h is greater than $0.5T_m$, the creep deformation will be the dominate deformation mode in metallic materials [26]. Solders have extremely high homologous temperatures even at room temperature due to their low melting temperature. T_h of Sn–Pb eutectic is $0.65T_m$ at room temperature ($T_m = 183$ °C), while the T_h of SAC alloys is $0.61T_m$ at room temperature ($T_m = 217$ °C). Both of these homologous temperatures are greater than $0.5T_m$, and so are considered "hot" at room temperature. Consequently, solder alloys will undergo creep even at room temperature. In actual electronic applications, where circuits typically operate over a −40 °C to +125 °C range, eutectic solder is working at 0.51–0.87T_m, while an SAC solder is working at 0.48–0.81T_m. Both of these ranges are within the rapid creep deformation range when devices are under stress.

Creep and creep curves

Creep generally refers to the time-dependent strain plastic deformations at constant uniaxial stress [27]. Creep deformation tends to be rapid when the homologous temperature is above $0.5T_m$. Creep testing can be carried out with a constant load at elevated temperature by either tension or compression [28].

Figure 10 shows a typical creep curve, which generally consists of three stages after the initial instantaneous strain when a constant load is applied [27]. The initial strain may consist of elastic or time-independent plastic deformation

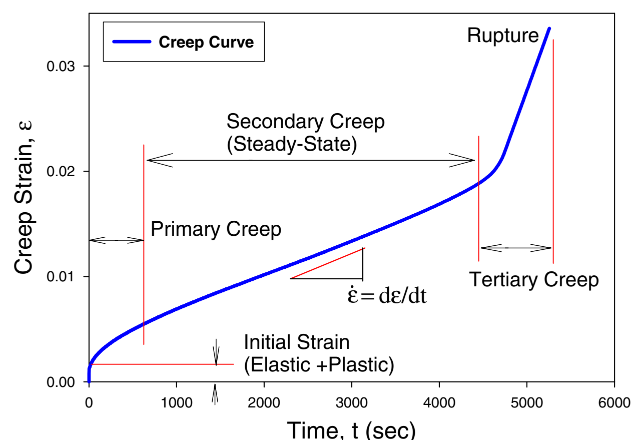

Fig. 10 Typical creep curve of lead-free solders

as soon as the load is applied. In this first stage, which is referred to as *Primary Creep*, the strain rate decreases rapidly over time. This is caused by work hardening, which restricts the deformation. Stage two is the *Secondary Creep*, or *Steady-State Creep*, which is very important since most of the plastic deformation and lifetime of products takes place in this period, and it is the dominant deformation for metals when the homologous temperature is above $0.5T_m$. In this stage, the strain rate is retarded by strain-hardening, which decreases the deformation speed, while the associated recovery and recrystallization (softening) tend to accelerate the creep rate [18]. The two processes of hardening and softening achieve a dynamic balance in the secondary creep stage and the strain-rate is relatively stable. The third stage is *Tertiary Creep*, where the nucleation and growth of cavities has been induced [27]. Necking and micro-cracking will subsequently occur, which will eventually lead to creep rupture of the specimen.

Mechanisms of creep deformation for solder alloys

Many creep mechanisms have been proposed. The major creep mechanisms, such as dislocation glide, dislocation creep, grain boundary diffusion, and lattice diffusion, can be summarized in a creep deformation map, as shown in Fig. 11 [27, 28]. The deformation diagram was first introduced by Ashby in 1972 [29], and has been widely accepted and studied by other researchers in the area. The deformation map is normally constructed with axes of normalized tensile or shear stress and homologous temperature. The top of the map is bounded to the theoretical or ideal stress, below which is the onset of dislocation

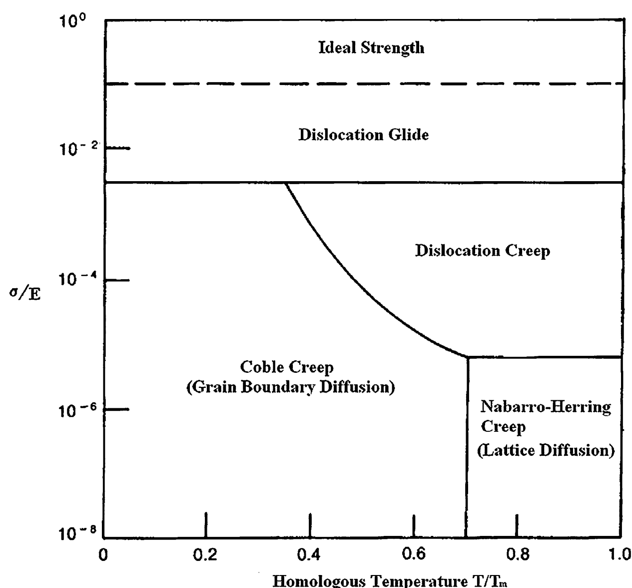

Fig. 11 Creep deformation map of solder alloys [27, 28]

glide. *Dislocation glide* occurs at high stress levels over the entire homologous temperature range. The deformation mechanism involves the dislocation moving along the slip planes [28]. *Dislocation creep* usually occurs at high temperatures, with T_h greater than $0.5T_m$, and intermediate high stress. This creep mechanism was first introduced by Weertman [30]. The deformation is believed to be controlled by diffusion controlled dislocation movement, with dislocations climbing away from dislocation barriers. This model is important because it can actually predict the strain rate through quantitative estimation. Coble proposed a *grain boundary based diffusion* mechanism, which involves the atomic or ionic diffusion along the grain boundaries [31]. The deformation occurs at intermediate low stress levels over an intermediate to low temperature range.

At low stress level and high temperature, *lattice or bulk diffusion* is believed to be the primary deformation mechanism [18]. This is also known as Nabarro-Herring Creep, since it was first reported by Nabarro and Herring independently [18, 32, 33]. The deformation is believed to involve the migration of interstitial atoms and lattice vacancies along the gradient of a grain boundary in the presence of tension or compression pressure in reversed directions. When there is no pressure the interstitial atoms and lattice vacancies will migrate proportional to the gradient of their concentrations. However, under pressure these lattice defects tend to move in whichever direction will relieve the imbalance of pressure, which will eventually cause creep deformation [33].

At high temperatures, grain-boundary sliding may also be involved in the creep deformation [18]. The displacement of grains can be induced by stress at high temperatures. Grain boundary sliding is not an independent deformation mechanism, but may accompany one or more of the above deformation mechanisms.

Solder alloys possess high homologous temperatures greater than $0.5T_m$ in their typical operating range. The creep deformation mechanism depends mainly on the stress level. At lower stress levels, the deformation will be due to lattice diffusion and grain-boundary diffusion; at intermediate stress levels dislocation creep is involved; and at high stress creep involves dislocation gliding.

Shi et al. recently proposed a new set of deformation maps for Sn–Pb eutectic solder [34]. It is believed that dislocation-controlled and lattice diffusion-controlled creep is the major deformation mode for eutectic solder.

Constitutive equations of secondary creep

Secondary, or steady-state creep is the dominant deformation experienced by solder alloys. The steady-state creep rate can be quantitatively estimated, and a series of

constitutive models have been proposed. The following two models are the most widely accepted for the characterization of solder alloys by considering the diffusion controlled creep deformation mechanism.

Dorn Power Law [35]:

$$\dot{\varepsilon} = A\sigma^n \exp\left(-\frac{Q}{RT}\right) \quad (6)$$

Garofalo Hyperbolic Sine Law [27]:

$$\dot{\varepsilon} = C[\sinh(\alpha\sigma)]^n e^{\left(\frac{-Q}{RT}\right)} \quad (7)$$

where R is the universal gas constant, T is the temperature in Kevin, σ is the applied stress, A and C are material dependent constants, n is the stress exponent, and Q is the activity energy. The models show that the steady-state creep strain rates are strongly stress and temperature dependent.

Data discrepancies in mechanical properties of lead-free solders

Data discrepancies in the literature

Due to the continuous pressure of the EU's WEEE and RoHS directives to ban lead-free solders from electronic components, research and development into lead-free solders have attracted more and more attention from both industry and academic institutions. Inputting the key words "lead-free solder" to the "Google" searching engine resulted in 162,000 links in March 2005, increasing to 1.44 million by September 2006. There are numerous technical research reports and articles in the area of mechanical characterization of lead-free solders. However, due to a lack of uniform standards and the uniqueness of the properties of the solder alloys, there are large discrepancies in the current database of the mechanical properties of lead-free solders.

Solder joint fatigue is one of the predominant failure mechanisms in electronic assemblies exposed to thermal cycling. Reliable, consistent, and comprehensive solder constitutive equations and material properties are needed for mechanical design, reliability assessment, and process optimization. Accurate mechanical characterization of solder materials has always been hampered by the difficulty of preparing test specimens that accurately reflect the material used in the actual solder joints (i.e., that match the solder microstructure). Solder uniaxial samples have generally been fabricated by either machining the bulk solder material [36–41] or by melting the solder paste in a mold [42–50]. Using bulk solder bars is undesirable because they will have significantly different microstructures than those present in the small solder joints used in microelectronics assembly. Machining can develop internal/residual stresses in the specimen, and the heat generated during turning operations can cause significant microstructural changes due to the low melting temperatures of solder alloys, which will cause a further deviation of mechanical properties. Reflow of solder paste in a mold leads to challenges with flux removal, minimization of voids, microstructure control, and extraction of the sample from the mold. Many of the approaches also lead to specimens with shapes that significantly deviate from the ideal long slender rods. Thus, undesired non-uniaxial stress states will inevitably be produced during loading.

Other investigators have attempted to extract the constitutive properties of solders by directly loading [40, 51–58] or indenting [54, 59] actual solder joints such as flip chip solder bumps or BGA solder balls. While such approaches are attractive because the true solder microstructure is involved, the unavoidable non-uniform stress and strain states in the joint make the extraction of the correct mechanical properties or stress–strain curves from the recorded load-displacement data very challenging.

The mechanical properties of most metals are both strain rate and temperature dependent [18]. The mechanical properties of solder alloys are heavily dependent on temperature and strain rate due to their high homologous temperature. Unless the testing conditions for both temperature and strain rate are the same, the data will not be comparable. The lack of testing standards thus makes it very hard to compare the data in the current data pool since different research groups use different specimen preparation methods and different testing conditions, such as strain rates and temperatures.

Table 2 provides a summary of the mechanical properties in the current research database of the major lead-free solders. All the data in the table were recorded at room temperature. There are large discrepancies in the tensile property values as well as the specimen preparation and testing approaches. The elastic modulus for SAC ranges from 30 to 54 GPa, although the majority of the values lie in the range of 40–50 GPa (Fig. 12). The UTS values vary from 30 to 60 MPa, with the majority in the range of 35–45 MPa (Fig. 13). The yield stresses range from 20 to 47 MPa, with the majority in the range of 25 to 35 MPa (Fig. 14).

All the differences in testing conditions, such as specimen geometry, testing methods, and testing strain rates, are likely to contribute to the variations. Vianco's SAC mechanical properties have been widely referenced [22, 60–62]. Figure 15 shows the bulk specimen used for compression testing in their experiment. As mentioned earlier, due to the low melting temperature of solder alloys, machining operations will cause significant changes in the microstructure and properties of solders. Residual stresses

Table 2 Tensile properties of SAC alloys

Solder alloy	Elastic modulus, *E* (GPa)	UTS (MPa)	YS (MPa)	Strain rate (s^{-1})	Specimen preparation	Testing method	Reference sources
Sn–3.9Ag–0.5Cu	50.3	36.2	31.9	4.2×10^{-5}	Machined, cylindrical	Compression	Vianco [22, 60–62]
	54				Machined, cylindrical	Dynamic/acoustic	Vianco [22, 60–62]
		60		1.78×10^{-3}	Cast, dog-bone, water quenched	Tension	Xiao [48, 49]
		41		1.78×10^{-3}	Aged 35 days at 25°	Tension	
Sn–3.8Ag–0.7Cu	43.1				Solder joints	Nano-indentation	Xu [109]
	45	40	35	6.68×10^{-4}	Cast, cylindrical	Tension	Hwang [36]
	50	45		1.67×10^{-3}	Cast, cylindrical	Tension	Fouassier [110]
	44.4	39.6	35.1	5.6×10^{-4}	Cast, dog-bone	Tension	Pang [68]
	46			10^{-4}	Cast, dog-bone	Tension	Schubert [23, 63]
	44.9				Solder joints	Nano-indentation	Li [111]
	41	39	32	10^{-3}	Cast, dog-bone	Tension	Lin [45]
	46		47.1		Solder joints	Dynamic analyzer	Harrsion [112]
Sn–4.1Ag–0.5Cu	43	36	33	6.86×10^{-4}	Cast, cylindrical	Tension	Hwang [36]
Sn–4.0Ag–0.5Cu	40				Cast, dog-bone	Tension	Schubert [23]
	48.3				Solder joint	Nano-indentation	Rhee [113]
	45				Bulk solder	Nano-indentation	Allen [114, 115]
		51		10^{-3}	Cast, dog-bone	Tension	Xiao [116]
Sn–3.0Ag–0.5Cu	54	41.8	25.3	4×10^{-3}	Machined, cylindrical	Tension	Kanchano-mai [69]
	37.4	43	37	5×10^{-4}	Cast, dog-bone	Tension	Zhu [117]
Sn–3.1Ag–0.5Cu	45	49	40	6.86×10^{-4}	Cast, cylindrical	Tension	Hwang [36]
Sn–3.2Ag–0.8Cu		32	28		Cast, cylindrical quenched	Tension	Medini [118]
		30	20		Air-cooled		
Sn–3.5Ag–0.7Cu		46.6			Cast, dog-bone	Tension	Schubert [23]
							Biglari [64]
SAC1[a]	30	38.1	28		Cast, cylindrical	Tension	AIM solder guide [119, 120]
SAC2[a]	51	39.5	33.5		Cast, cylindrical	Tension	AIM solder guide [119, 120]

[a] The solder composition was not specified

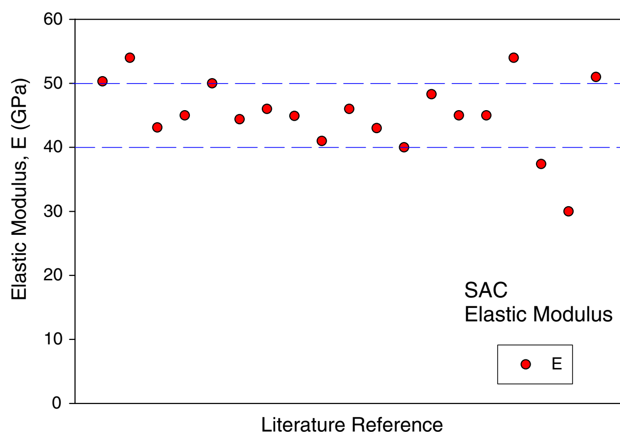

Fig. 12 Variations in the elastic modulus of SAC solders

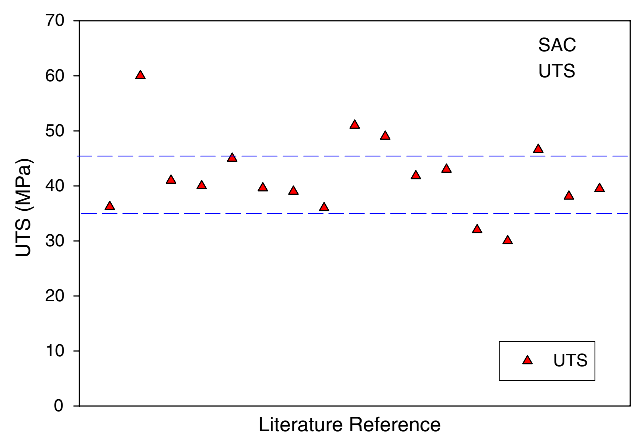

Fig. 13 Variations in the UTS for SAC solders

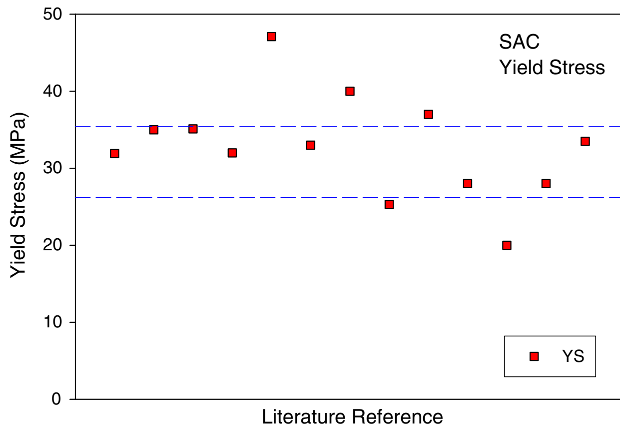

Fig. 14 Variations in the of yield stress for SAC solders

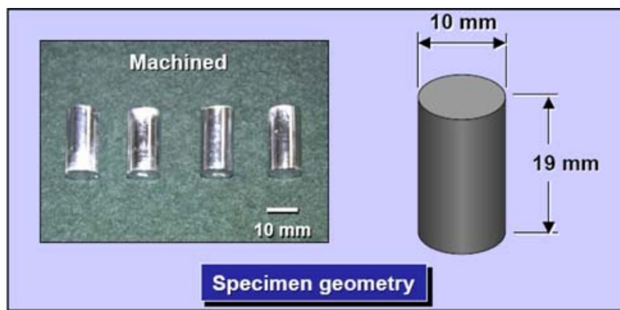

Fig. 15 Machined cylindrical solder specimen for compression testing [61]

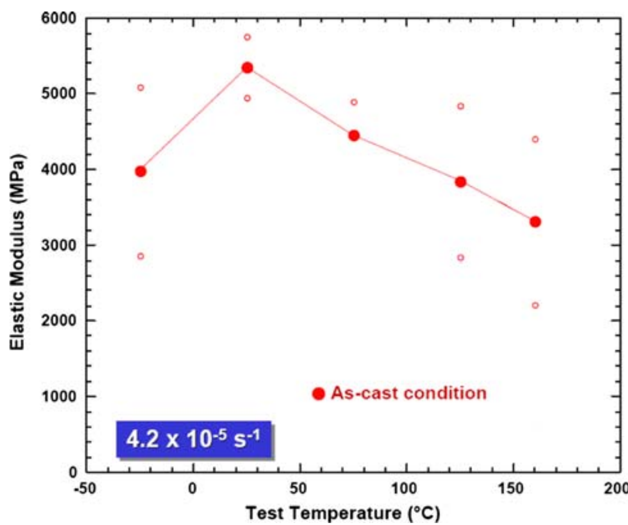

Fig. 16 The elastic modulus of SAC Solders by compression testing [61]

due to machining will also be significant. Their research used compression testing, which may pose problems due to confinement issues affecting the uniaxial testing results. Their results, shown in Fig. 16, seem to be abnormal with the changes of testing temperature [61], and their testing

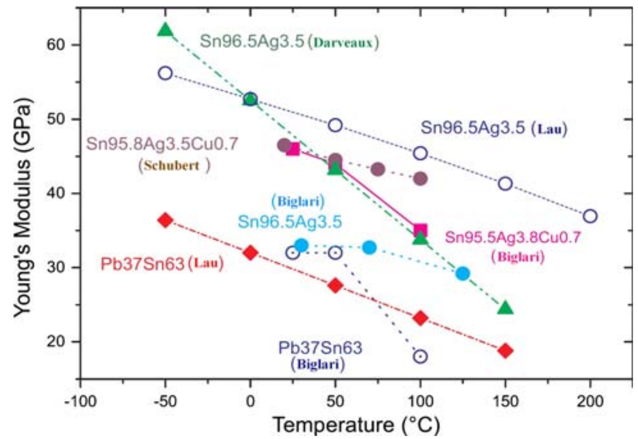

Fig. 17 Schubert's comparison of the elastic modulus of lead-free solders [23]

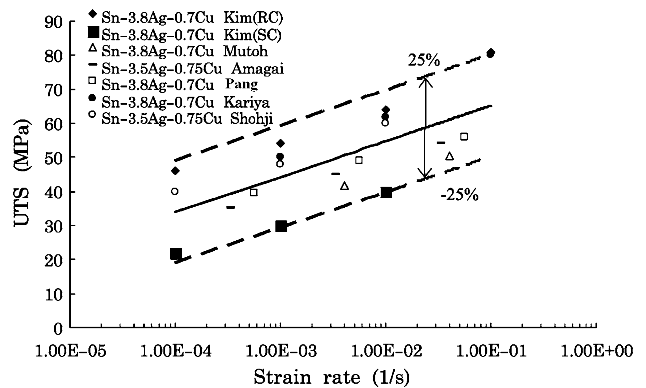

Fig. 18 Pang's comparison of the UTS of lead-free solders [68]

results show large deviations across all the temperatures tested in their testing data.

As shown in Fig. 17, Schubert et al. concluded that there are large discrepancies for the elastic modulus of both lead-free solders and Sn–Pb eutectic from different research reports due to variations in the testing conditions [23, 63–67]. Pang et al. found that there are about 50% of variations in the UTS values for SAC alloys (Fig. 18) [68–73].

Table 3 gives a brief summary of the mechanical properties of Sn–Pb eutectic solders. The collected data show there are also large variations in the mechanical properties published for eutectic Sn–Pb solder, with the elastic modulus ranging from 16 to 36 GPa, the UTS values ranging from 26 to 47 MPa, and the Yield stress ranging from 27 to 41 MPa. MacCabe and Fine reviewed the elastic modulus of Sn-eutectic solders and found a wide range, varying from 15 to 40 GPa [24]. They concluded that the large differences were caused by the contribution of the inelastic deformation (plastic) from the slope of the stress–strain curve due to the high homologous temperature of solders. The slope of the stress–strain curve therefore does not represent the true elastic modulus.

Table 3 The tensile properties of Sn–37Pb eutectic solder

Solder alloy	Elastic modulus, *E* (GPa)	UTS (MPa)	YS (MPa)	Strain rate (s^{-1})	Specimen preparation	Testing method	References sources
Sn–Pb eutectic	33.5	33.9	30.2		Cast, cylindrical	Tension	Seelig [119]
	27	47	41	6.86×10^{-4}	Cast, cylindrical	Tension	Hwang [36]
	32	39		1.67×10^{-3}	Cast, cylindrical	Tension	Fouassier [110]
	32		32.5		Solder joints	Dynamic analyzer	Harrison [112]
	36	54		2×10^{-2}	Lap-joints	Tension/shearing	Enke [121]
	35	26		10^{-3}	Machined, cylindrical	Tension	MacCabe [24]
	29		29				Lau [65]
	15.7	30.6	27.2				NCMS [122]
	32.1						Lau [123]
	30.2						Wong [124]
		31–46					Sigolko [125]
		46.2					Welco Casting [126]
		40.3					Hernadez [127]

As the above data show, there are large discrepancies in the current database of mechanical properties for both lead-free and Sn–Pb solders. These discrepancies may have been caused by the lack of accepted standards for testing methods, specimen preparation, and testing conditions. However, none of the resources recognized the effect of room temperature aging, which may also lead to data variations even for the same testing conditions due to the high homologous temperature of solder alloys. The room temperature aging effects may have played a significant role in the discrepancies in the published data.

Isothermal aging effects

The effects of aging on the mechanical properties and microstructure have been widely studied. However, most of the research has focused on elevated thermal aging effects, which dramatically change the mechanical properties and microstructure of solders. Room temperature aging effects have been largely ignored.

Effects of aging on tensile properties

The microstructure, mechanical response, and failure behavior of lead-free solder joints in electronic assemblies are constantly changing when exposed to isothermal aging and/or thermal cycling environments [46, 48, 49, 55, 56, 74–88]. The observed material behavior variation during thermal aging/cycling is universally detrimental to reliability and includes reductions in stiffness, yield stress, ultimate strength, and strain to failure, as well as highly accelerated creep. Such aging effects are greatly exacerbated at the higher temperatures that are typically used in thermal cycling qualification tests. However, significant changes occur with aging even at room temperature [46, 48, 49, 55, 56, 74–82].

As early as 1956, Medvedev [74] observed a 30% loss of tensile strength for bulk Sn/Pb solder stored for 450 days at room temperature. In addition, he reported 4–23% loss of tensile strength for solder joints subjected to room temperature storage for 280–435 days. In 1976, Lampe [75] found losses in shear strength and hardness of up to 20% in Sn–Pb and Sn–Pb–Sb solder alloys stored for 30 days at room temperature (Fig. 19). Lampe explained that the softening at room temperature due to aging was caused by the equilibrium process of the solder as tin precipitated out of the supersaturated lead-rich phase, thus causing the reduction in strength [75].

Miyazawa and Ariga [76, 77] measured significant hardness losses and microstructural coarsening for Sn–Pb, Sn–Ag, and Sn–Zn eutectic solders stored at 25 °C for 1000 h, while Chilton and co-workers [78] observed a 10–15% decrease in the fatigue life of single SMD joints after

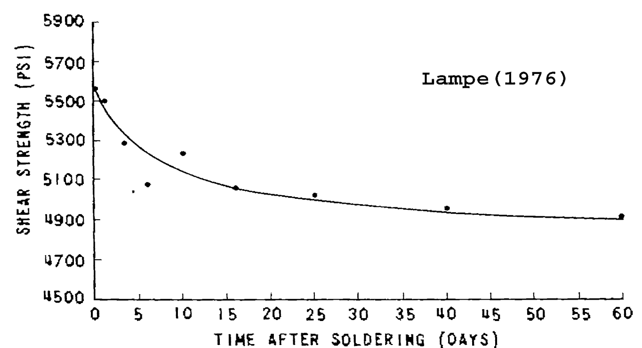

Fig. 19 Room temperature aging effects on Sn–Pb solders [75]

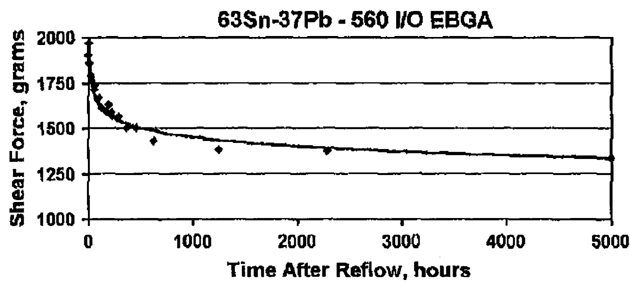

Fig. 20 Shear strength of BGA solder balls after 240 h at room temperature [80]

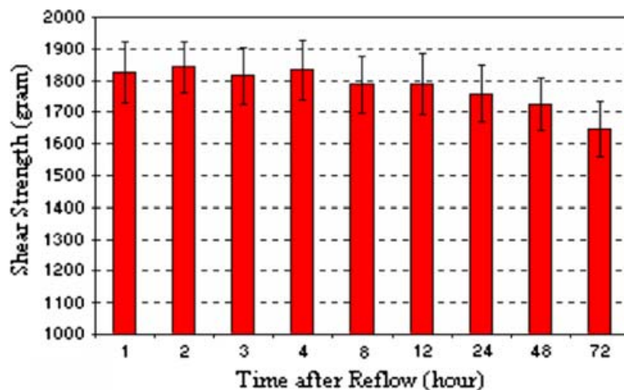

Fig. 21 Reduction in ball shearing strength after 3 days at RT [82]

room temperature aging. Coyle et al. reported a shearing stress reduction of up to 20% after 240 h at room temperature for BGA packaging (Fig. 20) [80]. Lee et al. also found that the shearing stress dropped by up to 10% after 3 days room temperature aging after reflow (Fig. 21) [82].

Several other studies [79, 81] have also documented the degradation of Sn–Pb and SAC solder ball shear strength (10–35%) in area array packages subjected to room temperature aging. Both Lampe and Coyle et al. observed dramatic coarsening of the phase microstructure [75, 80]. The effects of room temperature isothermal aging on constitutive behavior have also been reported [46, 48, 49]. Chuang et al. [46] characterized the reductions in yield stress and increases in elongations obtained in Sn–Zn eutectic solder during aging at room temperature. In addition, Xiao and Armstrong [48, 49] recorded stress–strain curves for SAC 396 specimens subjected to various durations of room temperature aging, and finding losses of ultimate tensile strength of up to 25% over 60 days of room temperature aging.

Thermal aging effects are the most widely studied due to the dramatic changes in the microstructure and mechanical properties that result. Aging softening has also been observed for solder subjected to elevated temperature aging (e.g., 125 °C) [45, 46, 48, 49, 83–88]. Pang et al. [55] measured microstructure changes, intermetallic layer growth, and shear strength degradation in SAC single ball joints aging at elevated temperature.

Darveaux [56] performed an extensive experimental study on the stress–strain and creep behavior of area array solder balls subjected to shear. He found that aging for 1 day at 125°C caused significant changes in the observed stress–strain and creep behavior. In addition to the room temperature aging experiments described above, Xiao and Armstrong also measured stress–strain curves for SAC 396 specimens subjected to elevated temperature aging at 180 °C [48, 49]. At this highly elevated temperature, they observed a quick softening of the material during the first 24 h, followed by a gradual hardening with time. Several studies have been performed on the degradation of BGA ball shear strength with elevated temperature aging at 125 °C or 150 °C [83–87]. All of these investigations documented both microstructure coarsening and intermetallic layer growth. In addition, Hasegawa et al. [83] measured elastic modulus reductions with aging by testing thin solder wires. Wang et al. [87] found significant drop in tensile properties after aging at 125 °C for various periods of time. Vianco also found large reductions in the elastic modulus and yield stress after thermal aging at 125 °C for 24 h for SAC alloys [22, 60–62]. Ding et al. [88] explored the evolution of fracture behavior of Sn–Pb tensile samples with elevated temperature aging.

Recently, Ma et al. of Auburn University has discovered that up to 40% reduction in tensile strength was observed after 2 months of aging at room temperature [89]. Room temperature aging also significantly deteriorated the creep resistance of both lead-free and Sn–Pb solders. Creep deformation increased dramatically with the increasing of aging durations. Microstructural changes during room temperature aging have also been observed and recorded for the solder alloys and correlated with the observed mechanical behavior changes. Our results on room temperature aging effects would provide the baseline database for the further study in the properties of both lead-free and lead containing solders, such as aging and elevated temperature, strain rate and temperature effects, and the constitutive modeling of creep.

The underlying mechanism for this reduction in strength in solder alloys after aging must be related to the microstructure coarsening process. When the grain structure is coarser, there are fewer grain boundaries to block the dislocation movement, causing a loss of strength of the material. Based on experimental data, Hall and Petch independently found that the yield strength of a polycrystalline material is inversely proportional to its grain size [18, 90, 91], as shown in Eq. 8:

$$\sigma_y = \sigma_i + kd^{-0.5} \quad (8)$$

where σ_y is yield strength of the polycrystalline material; σ_i is the constant for the material, which represents the overall resistance of the lattice to dislocation movement; k is a

constant which measures the contribution of hardening due to grain boundaries; and d represents the grain size. The Hall-Petch theory states that increasing grain size degrades the strength of materials. The increasing grain size will cause the amount of grain boundaries to decrease, and with fewer grain boundaries to resist the movement of dislocations the hardening contribution due to grain boundaries will be diminished, and the material loses strength.

The grain and phase structure coarsening is promoted by the self-diffusion of atoms, interstitials, and vacancies. According to the diffusion fundamental equation (Eq. 9) [19],

$$D = D_0 \exp\left(-\frac{Q}{RT}\right) \quad (9)$$

where D is diffusivity, D_0 is a constant that is independent of temperature, R is the Boltzmann constant, Q is the activation energy, and T is the absolute temperature. Higher temperatures will increase the diffusivity of the atoms, interstitials, and vacancies, leading to grain growth.

As previously stated in "General review of lead-free solders and the mechanical properties of lead-free solders" section, the elastic modulus is only related to the interatomic forces between adjacent atoms [18]. Under normal conditions, the atoms reach an equilibrium position to balance the attraction and repulsion forces. When an external force is applied within the elastic region, no interatomic bonds are broken, and only the balance of the attraction and repulsion forces changes. When the external force is relieved, the atoms will return to their original equilibrium positions. Consequently, microstructural changes have little effect on the value of the true modulus. However, in engineering practice, the apparent elastic modulus is obtained from the slope of the stress–strain curves and includes time-dependent inelastic deformations such as creep. Creep is strongly dependent on the dislocation movement and grain size. Coarser grains will cause more grain gliding and dislocation movement, and thus lead to more severe creep deformation. The contribution of plastic deformation to the apparent elastic modulus will therefore increase with increasing grain size. This explains why isothermal aging can cause a reduction in the apparent elastic modulus. Due to the high homologous temperature of solder alloys even at room temperature, creep deformation is more significant compared to other metals with higher melting temperature. The aging effects also contribute more to the apparent elastic modulus for solder alloys.

Effects of aging on creep

No reports on the effects of room temperature aging on creep deformation were found. All the current research reports have focused solely on the effect of elevated temperatures on creep deformation. It is believed that thermal aging accelerates the creep deformation due to the growth of the grain structure and coarsening of the second phase in lead-free solders. Darveaux found that aged specimens creep much faster than unaged ones by a factor of up to 20 times after aging at 125 °C for 24 h for both SAC405 and SAC305 solder alloys (Fig. 22) [56]. Note, however, that the lap shear joint specimens used in Darveaux's tests may create non-uniform stress and strain states in the specimens. Several other studies have observed similar behavior regarding the aging deterioration of creep deformation [22, 48, 92–94].

Sasaki et al. found that bulk specimens after thermal cycling experience a much higher creep deformation rate [95].

Ma et al. also investigated the effects of elevated temperature aging up to 6 months [96]. Aging at elevated temperature has been found to have much more significant effects on the mechanical properties and microstructure evolution than that of the room temperature aging. The thermal aging has caused significant tensile strength loss and deterioration of creep deformation. The thermal aging results also showed that after initial tensile strength drop,

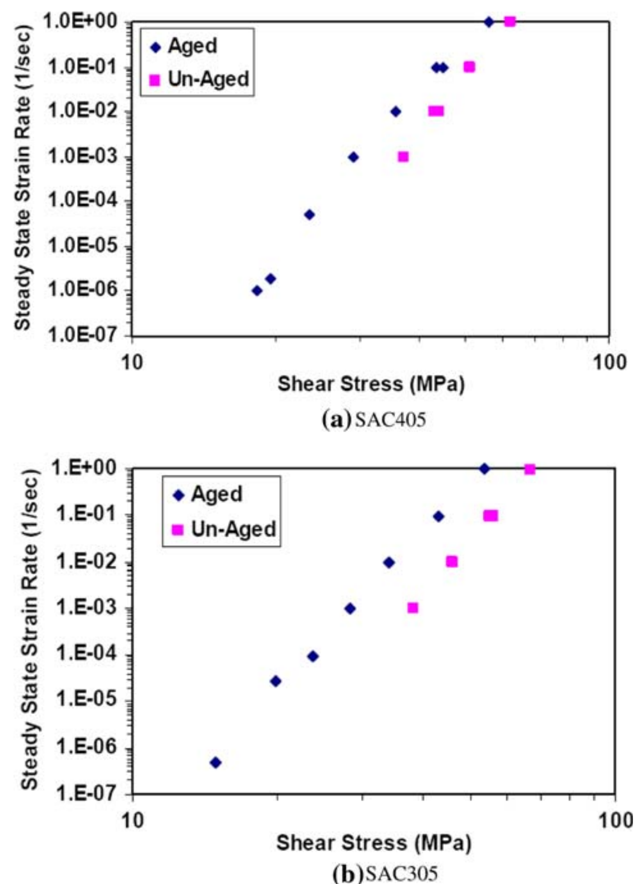

Fig. 22 Effects of thermal aging on creep deformation of SAC solders [56]

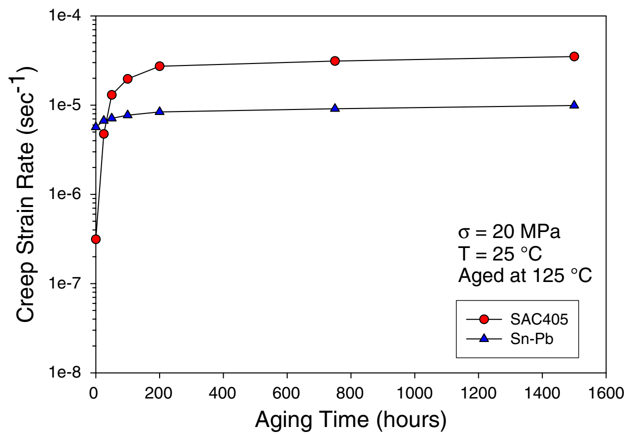

Fig. 23 Comparison of Sn–Pb and SAC creep rates for aging at 125 °C [96]

the Sn–Pb eutectic solder reached a relative stable stage after 200 h of aging. However, for SAC alloy, both the tensile and creep properties continuously change with the increasing of aging time. It is noteworthy that the creep deformation of SAC alloy is only better than Sn–Pb at room temperature and shorter aging time. There is a crossover point at about 50 h of aging at 125 °C (Fig. 23). The creep resistance of SAC alloy was lower than that of Sn–Pb at longer aging durations. So lead-free solder reliability need to be carefully analyzed especially after aging.

Effects of strain rate and temperature on tensile properties

Mechanical properties are temperature and strain rate dependent for most metal alloys, especially for metals with low melting and high homologous temperatures. High temperatures induce transitions in macroscopic fracture, and these transitions parallel the changes in the strength and ductility of materials [18]. Materials lose strength at higher temperatures. Hertzberg stated that the material strength increases with the testing strain rate, following a form similar to Holloman's Equation [18]:

$$\sigma = C\dot{\varepsilon}^{m} \tag{10}$$

where m is the strain-rate sensitivity factor, or strain hardening exponent; $\dot{\varepsilon}$is the strain rate; C is the material constant; and σ is the stress.

Solder alloys possess very high homologous temperatures. The properties of solder alloys are strongly dependent on both the temperature and strain rate. Jones et al. have observed an approximately linear relationship between the strength and temperature [97, 98]:

$$\sigma = -\alpha T + \beta \tag{11}$$

where α is temperature strengthening coefficient; β is the strength at 0 °C in MPa, and T is the testing temperature in °C. Pang, Shi, and co-workers have observed similar experimental results, with a near linear relationship with temperature and a power law relation (Eq. 10) with the strain rate [39, 99]. Several other studies have also observed similar materials behavior for both Sn–Pb eutectic and lead-free solder alloys [100–103].

Constitutive modeling of creep deformation

Constitutive modeling of creep deformation has been a heavily studied and researched area due to the importance of being able to predict the end of life of electronic packaging using finite element analysis tools. Many models have been proposed and modified by researchers. As mentioned in previous section, the Dorn power law and Garofalo Hyperbolic models are the most widely accepted models for solder alloys. The constitutive model can be determined by creep testing at different temperature and stress levels. Tables 4 and 5 summarize some of the current data for both lead-free solder alloys and Sn–Pb; all the models are based on steady-state creep. Materials constants, specimens, and testing methods are compared in the tables. The majority of the data can be fitted into the Hyperbolic Sine model. As with the testing of tensile properties, there are large discrepancies in the creep data and material constants vary over a very large range. The materials constants are important in determining the accuracy of end-of-life prediction for solder joints using finite element analysis. Large discrepancies would degrade the accuracy of these predictions.

Figure 24 summarize several of the hyperbolic sine models for SAC alloys at 125 °C, showing how the steady-state creep rate varies over a very large range. Clech reviewed creep modeling for both Sn–Pb and lead-free solder alloys based on the currently available data under a NIST project [104], and commented that the current database are widely scattered. Discrepancies may be caused by differences in the specimen, testing method, and testing conditions and the possible effects of room temperature aging as highlighted before.

Both the Garofola Hyperbolic Sine model and Dorn Power Law model focus on steady-state creep data, which only involve the time dependent creep deformation. Recently, more research has been carried out to investigate the Anand model, which is also offered in the ANSYS code. The Anand model was initially proposed by Anand [105], and is considered to be a unified model that does not require explicit yield conditions or loading/unloading criteria. The instantaneous response of the material is dependent on its current state. The Anand model also employs a single scalar internal variable "s" to represent

Table 4 Garofalo hyperbolic creep models of solder alloys

Constitutive models	Solder alloy	Constants				Specimen testing method	Reference sources
Garofalo hyperbolic Sine Law		C	α (MPa^{-1})	n	Q (kJ/mol)		
$\dot{\varepsilon} = C[\sinh(\alpha\sigma)]^n e^{\left(\frac{-Q}{RT}\right)}$	Sn–40Pb	0.1114	751	3.3	53.0	Lap-joints, shear/tensile	Darveaux [128]
	Sn–37Pb	0.158	0.406	1.38	50.0	Cast bulk, tensile	Xiao [129]
		10.0	0.1	2	44.9	Flip chip joints, tensile	Wiese [23]
		2.87×10^{-5}	1300	3.3	52.8		Shi [34]
		1999.4	0.2	2.1	54.1	Lap-joint, tensile	Zhang [130]
	Sn–3.5Ag	178.5	0.115	4.75	57.1	Bulk, tensile	Wiese [23]
		23.17	0.0509	5.04	41.6	Bulk, tensile	Clech [104]
		8.18×10^{11}	0.0266	8.67	77.4	Lap joint, shear	Clech [104]
		2.46×10^{5}	0.0913	5.5	72.5	Lap joint, shear	Clech/Darveaux [66, 104]
	Sn–3.0Ag–0.5Cu	2631	0.0453	5.0	52.4		Vianco [22]
	Sn– 3.9Ag– 0.6Cu	0.184	0.221	2.89	62.0	Cast bulk, tensile	Xiao [129]
		4.41×10^{5}	0.005	4.2	45	Bulk, compression	Lau & Vianco [131]
		3.49×10^{4}	0.005	4.3	43.13	Bulk, compression	Vianco [61]
		248.4	0.188	3.79	62.3	Lap-joint, tensile	Zhang [130]
	Sn–3.8Ag–0.7Cu	3.2×10^{4}	0.037	5.1	65.3	Bulk, tensile	Pang [132]
		2.78×10^{5}	0.0245	6.41	54.2		Schubert [133]
	SAC series	7.93×10^{5}	0.0356	5	67.9	Fitting data	Clech [104]

Table 5 Dorn power law creep models of solder alloys

Constitutive models	Solder alloy	Constants			Specimen testing method	Reference sources
Dorn power law		A (s^{-1})	n	Q		
$\dot{\varepsilon} = A\sigma^n \exp\left(-\frac{Q}{RT}\right)$	Sn–3.5Ag	5×10^{-6}	11	79.8	Flip chip, tensile	Wiese [23]
		9.44×10^{-5}	6.05	61.1	Bulk, tensile	Clech [104]
	Sn–4.0Ag–0.5Cu	2×10^{-21}	18	83.1	Flip chip, tensile	Wiese [23]

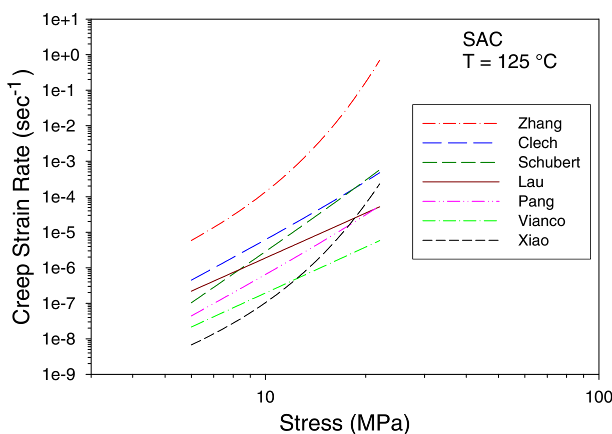

Fig. 24 Discrepancies in the creep models

the isotropic resistance to inelastic flow of the material. There are series of equations for the Anand model. The flow equation is expressed as follows:

$$\dot{\varepsilon}_P = A\left[\sinh\left(\frac{\xi\sigma}{s}\right)\right]^{\frac{1}{m}} \exp\left(-\frac{Q}{RT}\right) \tag{12}$$

where $\dot{\varepsilon}_p$is the inelastic strain rate, A is a constant, ξ is the stress multiplier, σ is the stress, R is the gas constant, m is the strain rate sensitivity, Q is the activation energy and T is absolute temperature. The flow equation can be easily modified to represent the hyperbolic sine model for secondary creep rate (Eq. 7).

The scalar variable is believed to be related to the dynamic process of strain hardening and dynamic recovery, expressed as follows:

$$\dot{s} = \left\{\left[h_0\left|1 - \frac{s}{s*}\right|\right]\frac{\left(1 - \frac{s}{s*}\right)}{\left|1 - \frac{s}{s*}\right|}\right\}\dot{\varepsilon}_p \tag{13}$$

and

$$s^* = \hat{s}\left[\frac{\dot{\varepsilon}_p}{A}\exp\left(\frac{Q}{RT}\right)\right]^n \tag{14}$$

where s^* represents a saturation value at a given temperature and strain rate, $\hat{s}$is a coefficient, and n is the strain rate sensitivity at the saturation condition.

There are a total of nine constants from the above equations, A, Q, m, n, a, h_0, ξ, $\hat{s}$, and s_0, the initial value of the deformation resistance, which need to be determined for the viscoplastic Anand model. Currently, most researchers use multiple variable fitting methods to determine the constants based on experimental data. However, as with the previously documented data, there are large variations in the current database for these constants, even for the same solder material under the same conditions [106–108].

Summary

This review of the research literature has documented the dramatic changes that occur in the constitutive and failure behavior of solder materials and solder joint interfaces during isothermal aging. However, these effects have been largely ignored in most previous studies involving solder material characterization or finite element predictions of solder joint reliability during thermal cycling. It is widely acknowledged that the large discrepancies in measured solder mechanical properties from one study to another arise due to differences in the microstructures of the tested samples. This problem is exacerbated by the aging issue, as it is clear that the microstructure and material behavior of the samples used in even a single investigation are moving targets that change rapidly even at room temperature. Furthermore, the effects of aging on solder behavior must be better understood so that more accurate viscoplastic constitutive equations can be developed for SnPb and SAC solders. Without such well-defined relationship, it is doubtful that finite element reliability predictions can ever reach their full potential.

Due the fundamental differences in microstructure and properties between traditional Sn/Pb solder and lead-free solders, great care needs to be taken in the conversion of lead-free solders. Recent researches showed that the aging effects will significantly decrease the mechanical properties of lead-free solders, and it is much severe than that of Sn/Pb solders. The current and future research need to pay particular attentions in long term aging effects in the implementation of lead-free solders, especially for high risk and infrastructure equipment which operate at harsh environment. In regard to developing new lead-free solders, the microstructure evolution and its impact to the mechanical and electrical properties to the solder joints during the product operating life need to be carefully examined.

References

1. Allenby BR, Ciccarelli JP (1992) In: Proceeding of surface mount international conference, pp 1–28
2. Turbini LJ (2001) IEEE Trans Electron Pack Manuf 24(1):4
3. Hwang JS (2004) Implementing lead-free electronics. McGraw-Hill, New York, NY, p 1
4. Grusd A (1999) In: Proceedings of the technical program NEPCON west, pp 212–221
5. IPC Roadmap (2000) A guide for assembly of lead-free electronics. IPC, Northbrook, IL
6. Abtew M, Selvaduray G (2000) Mater Sci Eng 27:95
7. Zeng K, Tu KN (2002) Mater Sci Eng 38:55
8. Karlya Y, Gagg C, Plumbridge WJ (2000) Solder Surf Mt Technol 13:39
9. Lee NC (1997) Solder Surf Mt Technol 26:65
10. Soldertec (2002) European lead-free roadmap, ver 1, p 1
11. Deubzer O, Hamano H, Suga T (2001) In: Proceedings of the 2001 IEEE international symposium on electronics and the environment, pp 290–295
12. Nimmo K (2004) In: Suganuma K (ed) Alloy selection, chapter 3 of lead-free soldering in electronics: science, technology and environmental impact. Marcel Dekker, New York, p 61
13. Ye L, Lai ZH, Liu J, Thölén A (2001) Solder Surf Mt Technol 13:16
14. Iting T, Li JT, Yen SF, Chuang TH, Lo R, Ku T, Wu E (2005) In: Proceedings of the 55th electronic components and technology conference, pp 687–691
15. Fields RJ, Low SR. Physical and mechanical properties of intermetallic compounds commonly found in solder joints. Available online at: http://www.metallurgy.nist.gov/mechanical_properties/solder_paper.html
16. Ganesan S, Pecht M (2006) Lead-free electronics. Wiley-Interscience Publication, New York, p 51
17. Hwang J (2001) Environment-friendly electronics: lead free technology. Electrochemical Publications, British Isles, p 134
18. Hertzberg RW (1996) Deformation and fracture mechanics of engineering materials, 4th edn. Wiley, New York
19. Thornton PA, Colangelo VJ (1985) Fundamentals of engineering materials. Prentice-Hall, Inc, Upper Saddle River, NJ, p 227
20. Gilman JJ (1969) Micromechanics of flow in solids. McGraw-Hill, New York
21. Ralls KM, Courtney TH, Wulff J (1976) Introduction to materials science and engineering. Wiley, New York
22. Vianco PT (2006) In: Shangguan D (ed) Fatigue and creep of lead-free solder alloys: fundamental properties, chapter 3 lead-free solder interconnect reliability. ASM International, Materials Park, OH, p 67
23. Wiese S, Schubert A, Walter H, Dudek R, Feustel F, Meusel E, Michel B (2001) In: Proceeding of the 51st electronic components and technology conference, pp 890–902
24. McCabe RJ, Fine ME (1998) Scripta Mater 39(2):189
25. Lau JH, Pao YH (1997) Solder joints reliability of BGA, CSP, Flip-Chip, and Fine Pitch SMT assemblies. McGraw-Hill, New York
26. Cadek J (1988) Creep in metallic materials. Elsevier, Amsterdam
27. Garofalo F (1966) Fundamentals of creep and creep-rupture in metals. Macmillan, New York
28. Evans RW, Wilshire B (1985) Creep of metals and alloys. The Institute of Metals, New York
29. Ashby MF (1972) Acta Metall 20:887
30. Weertman J (1957) J Appl Phys 28:362
31. Coble RL (1963) J Appl Phys 34:1679
32. Nabarro FRN (1948) Report of a conference on the strength of solids. Physical Society, London, pp 75–81

33. Herring C (1950) J Appl Phys 21:437
34. Shi XQ, Wang ZP, Yang QJ, Pang HLJ (2003) J Eng Mater Technol 125:81
35. Mukherjee AK, Bird JE, Dorn JE (1969) Trans Am Soc Metal 62:155
36. Puttlitz KJ, Stalter KA (2004) Handbook of lead-free solder technology for microelectronic assemblies. Marcel Dekker, New York
37. Nose H, Sakane M, Tsukada Y, Nishimura H (2003) J Electron Packaging 125(1):59
38. McCormack M, Chen HS, Jin S (1994) Appl Phys Lett 65(10):1233
39. Shi XQ, Zhou W, Pang HLJ, Wang ZP (1999) J Electron Packaging 121(3):179
40. Pang JHL, Xiong BS, Neo CC, Zhang XR, Low TH (2003) In: Proceeding of the 53rd electronic components and technology conference, pp 673–679
41. Pang JHL, Xiong BS, Low TH (2004) Thin Solid Films 462–463:408
42. Yeung B, Jang JW (2002) J Mater Sci Lett 21:723
43. Kim KS, Huh SH, Suganuma K (2002) Mater Sci Eng A 333:106
44. Madeni JC, Liu S, Siewert T (2002) In: Proceedings of the ASM international conference
45. Lin JK, De Silva A, Frear D, Guo Y, Hayes S, Jang JW, Li L, Mitchell D, Yeung B, Zhang C (2002) IEEE Trans Electron Pack Manuf 25(4):300
46. Chuang CM, Liu TS, Chen LH (2002) J Mater Sci 37(1):191. doi:10.1023/A:1013143218738
47. Vianco PT, Rejent JA, Grant R (2004) Trans Jpn Inst Metall 45:765
48. Xiao Q, Nguyen L, Armstrong WD (2004) In: Proceedings of the 54th electronic components and technology conference, pp 1325–1332
49. Xiao Q, Bailey HJ, Armstrong WD (2004) J Electron Packaging 126(2):208
50. Shohji I, Yoshida T, Takahashi T, Hioki S (2004) Mater Sci Eng A366:50
51. Tsukada Y, Nishimura H, Yamamoto H, Sakane M (2005) J Electron Packaging 127(4):407
52. Yang H, Phillip D, Paul M, Murty KL (1996) In: Proceeding of 46th electronic components and technology conference, pp 1136–1142
53. Liu CY, Chen C, Mal AK, Tu KN (1999) J Appl Phys 85(7):3882
54. Rhee H, Subramanian KN, Lee A, Lee JG (2003) Sold Surf Mt Technol 15(3):21
55. Pang JHL, Low TH, Xiong BS, Xu L, Neo CC (2004) Thin Solid Films 462–463:370
56. Darveaux R (2005) In: Proceedings of the 55th electronic components and technology conference, pp 882–893
57. Obaid AA, Sloan JG, Lamontia MA, Paesano A, Khan S, Gillespie JW (2005) J Electron Packaging 127(4):483
58. Zhang Q, Dasgupta A, Nelson D, Pallavicini H (2005) J Electron Packaging 127(4):415
59. Chromik RR, Vinci RP, Allen SL, Notis MR (2003) JOM 55(6):66
60. Vianco PT, Rejent JA, Martin JJ (2003) JOM 55(6):50
61. Vianco PT, Rejent JA (2002) Compression deformation response of 95.5Sn–3.9Ag–0.6Cu solder, UCLA Workshop on Pb-free Electronics, 2002. Available at: http://www.seas.ucla.edu/eThinFilm/PbfreeWorkshop/pdf/vianco.pdf
62. Vianco PT, Rejent JA, Kilgo AC (2003) J Electron Mater 32(3):142
63. Schubert A, Walter H, Dudek R, Michel B, Lefranc G, Otto J, Mitic G (2001) In: International symposium on advanced packaging materials, pp 129–134
64. Biglari MH, Oddy M, Oud MA, Davis P (2000) In: Proceeding of electronics goes green 2000+ conference, pp 73–82
65. Lau JH, Pao Y-H (1997) Solder joint reliability of BGA, CSP, Flip Chip, and Fine Pitch SMT assemblies. McGraw-Hill, New York
66. Darveaux R, Banerji K, Mawer A, Dody G (1995) In: Lau JL (ed) Ball grid array technology. McGraw-Hill, New York, p 379
67. Lau JH, Chang C (1998) In: Proceeding of the 48th electronic component and technology conference, pp 1339–1344
68. Pang JHL, Xiong BS (2005) IEEE Trans Compon Pack Technol 28(4):830
69. Kanchanomai C, Miyashita Y, Mutoh Y (2002) J Electron Mater 31:456
70. Kim KS, Huh SH, Suganuma K (2002) Mater Sci Eng A 333:106
71. Amagai M, Watanabe M, Omiya M, Kishimoto K, Shibuya T (2002) Microelectron Reliab 42:951
72. Kariya Y, Plumbridge J (2001) In: 7th symposium on micro-joining and assembly in electronics, pp 383–388
73. Shohji I, Yoshida T, Takahashi T, Hioki S (2004) Mater Sci Eng A A366:50
74. Medvedev AS (1956) Metallovedenie i Obrabotka Metallov 7:16
75. Lampe BT (1976) Weld J 55(10):330s
76. Miyazawa Y, Ariga T (1999) In: Proceedings of the first international symposium on environmentally conscious design and inverse manufacturing, pp 616–619
77. Miyazawa Y, Ariga T (2001) Mater Trans Jpn Inst Metals 42(5):776
78. Chilton AC, Whitmore MA, Hampshire WB (1989) Sold Surf Mt Technol 3:21
79. Gagliano RA, Fine ME, Vaynman S, Stolkarts V (1999) In: Julia R (ed) Advanced materials for the 21st century: proceedings of the 1999. Weertman Symposium, pp 107–116
80. Coyle RJ, Solan PP, Serafino AJ, Gahr SA (2000) In: Proceedings of the 50th electronic components and technology conference, pp 160–169
81. Tsui YK, Lee SW, Huang X (2002) In: Proceedings of the 4th international symposium on electronic materials and packaging, pp 478–481
82. Lee SWR, Tsui YK, Huang X, Yan CC (2002) In: Proceedings of the 2002 ASME international mechanical engineering congress and exposition, pp 1–4
83. Hasegawa K, Noudou T, Takahashi A, Nakaso A (2001) In: Proceedings of the 2001 SMTA international, pp 1–8
84. Li M, Lee KY, Olsen DR, Chen WT, Tan BTC, Mhaisalkar S (2002) IEEE Trans Electron Pack 25(3):185
85. Chou GJS (2002) In: Proceedings of the 8th symposium on advanced packaging materials, pp 39–46
86. Law CMT, Wu CML (2004) In: Proceedings of HDP'04, pp 60–65
87. Wang Q, Johnson RW, Ma H, Gale WF (2005) In: 10th electronic circuit and world convention conference (ECWC 10)
88. Ding Y, Wang C, Li M, Bang HS (2004) Mater Sci Eng A384:314
89. Ma H, Suhling JC, Lall P, Bozack MJ (2006) In: Proceeding of the 56th electronic components and technology conference (ECTC), San Diego, CA, May 30–June 2, pp 849–864
90. Hall EO (1951) In: Proceedings of the physical society, vol 64, pp 747–753
91. Petch NJ (1953) J Iron Steel Inst 174:25

92. Lin J-K, Jang J-W, Hayes S, Frear D (2004) In: Proceeding of the 54th electronics packaging technology conference, pp 642–649
93. Wiese S, Meusel E, Wolter K-J (2003) In: Proceeding of the 53rd electronics packaging technology conference, pp 197–206
94. Banerji K, Darveaux R (1992) In: Proceeding of TMS-AIME symposium, pp 431–442
95. Sasaki K, Kobayashi T (2005) In: Proceeding of the ASME InterPACK'05
96. Ma H, Suhling JC, Lall P, Bozack MJ (2007) In: The proceeding of the 57th electronic components and technology conference (ECTC), pp 653–668
97. Jones WK, Liu Y, Zampino MA, Gonzalez G, Shah M (1997) Design and reliability of solders and solder interconnections, TMS
98. Jones WK, Liu Y, Zampino MA, Gonzalez G (1997) Adv Microelectron 24:30
99. Pang HLJ, Wang YP, Shi XQ, Wang ZP (1998) In: IEEE/CPMT electronics packaging technology conference, pp 184–189
100. Nose H, Sakane M, Tsukada T, Nishimura H (2003) J Electron Packaging 124:59
101. Plumbridge WJ, Gagg CR (1999) J Mater Sci: Mater Electron 10:461
102. Lang R, Tanaka H, Munegata O, Taguchi T, Narita T (2005) Mater Charact 54:223
103. Dai LH, Lee SR (2001) In: Proceeding of the ASME Inter-PACK'05, pp 307–313
104. Clech JP. Review and analysis of lead-free materials properties, NIST, Available at: http://www.metallurgy.nist.gov/solder/clech/Sn-Ag-Cu_Main.htm
105. Anand L (1985) Int J Plasticity 1:213
106. Pei M, Qu J (2005) In: International symposium on advanced packaging materials: processes, properties and interfaces, pp 45–49
107. Pang JHL, Low PTH, Xiong BS (2004) In: Proceeding of ITHERM'04, vol 2, pp 131–136
108. Rodgers B, Flood B, Punch J, Waldron F (2005) In: Proceedings of the 6th international conference on thermal, mechanical and multi-physics simulation and experiments in micro-electronics and micro-systems, pp 490–496
109. Xu L, Pang JHL (2005) In: Proceeding of the 55th electronics packaging technology conference, pp 357–362
110. Fouassier O, Heintz J-M, Chazelas J, Geffroy P-M, Silvaina J-F (2006) J Appl Phys 100:1
111. Li D, Liu C, Conway P (2004) In: Proceeding of the 54th electronic components and technology conference, pp 128–133
112. Harrison MR, Vincent JH, Steen HAH (2001) Solder Surf Mt Technol 13(3):21
113. Rhee H, Lucas JP, Subramanian KN (2002) J Mater Sci: Mater Electron 13:477
114. Allen SL, Notis MR, Chromik RR, Vinci RP (2004) J Mater Res 19:1417
115. Allen SL, Notis MR, Chromik RR, Vinci RP, Lewis DJ, Schaefer R (2004) J Mater Res 19:1425
116. Xiao L, Liu J, Lai A, Ye L, Tholen A (2000) In: International symposium on advanced packaging materials, pp 145–151
117. Zhu F, Wang Z, Guan R, Zhang H (2005) In: 2005 international conference on asian green electronics, pp 107–112
118. Madeni J, Liu S, Siewert T. Casting of lead-free solder bulk specimens with various solidification rates, NIST Pb-free data. Available at: http://www.boulder.nist.gov/
119. Seelig K, Suraski D (2000) In: Proceeding of the 50th electronic components and technology conference, pp 1405–1409
120. Lead-free soldering guide from AIM Solder Inc (2003) http://www.psma.com/ul_files/forums/leadfree/aim_lead_free_guide.pdf
121. Enke NF, Kilinski TJ, Schroeder SA, Lesniak JR (1989) IEEE Trans Compon Hybrids Manuf Technol 12(4):459
122. Technical reports for the lead free solder project: properties reports: room temperature tensile properties of lead-free solder alloys. Lead free solder project CD-ROM, National Center for Manufacturing Sciences (NCMS), 1998. Available at: http://www.boulder.nist.gov/
123. Lau JH, Chang C, Lee SWR, Chen TY, Cheng D, Tseng TJ, Lin, D (2000) In: Proceeding of NEPCON-west 2000, pp 554–562
124. Wong T, Matsunaga AH (1995) In: Proceeding of NEPCON west conference, 1995. Available at: http://www.boulder.nist.gov/
125. Sigelko JD, Subramanian KN (2000) Adv Mater Process 157(3):47
126. Welco Castings, Solder Data Sheet, 2 Hillyard Street, Hamilton, Ontario, Canada. Available at: http://www.boulder.nist.gov/
127. Hernandez CL, Vianco PT, Rejent JA (1998) Effect of interface microstructure on the mechanical properties of Pb-free hybrid microcircuit solder joints. IPC/SMTA Electronics Assembly Expo, pp S19-2-1. Available at: http://www.boulder.nist.gov/
128. Darveaux R, Banerji K (1992) IEEE Trans Compon Hybrids Manuf Technol 15(6):1013
129. Xiao Q, Armstrong WD (2005) J Electron Mater 34(2):196
130. Zhang Q, Dasgupta A, Haswell P (2003) In: Proceeding of the 53rd electronic components and technology conference, pp 1862–1868
131. Lau J, Dauksher W, Vianco P (2003) In: Proceeding of the 53rd electronic components and technology conference, pp 229–236
132. Pang JHL, Xiong BS, Low TH (2004) In: Proceeding of 54th electronic components and technology conference, pp 1333–1337
133. Schubert A, Dudek R, Auerswald E, Gollbardt A, Michel B, Reichl H (2003) In: Proceeding of the 53rd electronic components and technology conference, pp 603–610